DOI:10.34918/85116

Wesley Chebii RUTTO[1] , Benard KIPSANG[2,*]

Chapter 16. INVESTIGATION OF ADIPOSE MECHANICAL PROPERTIES UNDER COMPRESSION LOADING FOR IMPROVING HUMAN BODY ARMOR MODELING

To improve blast absorption characteristics of personal protection equipment (PPEs), understanding the effects of blasts on the human body itself is a critical step toward improving protective device design. Adipose tissue mechanical properties were investigated under quasi-static and dynamic compression loading at varying strain rates on specimens made from porcine subcutaneous adipose tissue. The specimens were subjected to a uniaxial compression test on an MTS universal testing machine to obtain stress versus strain response data. The tests were carried out at three strain rate regimes: 0.05%/s, 0.5%/s, and 5%/s. For modeling the passive behavior of subcutaneous adipose tissue, three-term QLV and one-term Ogden models were chosen. Python codes were used to numerically simulate experimental data. The hyperelastic material parameters obtained were as follows: $\mu = 16.4$, $\alpha = 8.41$, $C_1 = -136.980$, $C_2 = -225.60$, and $C_3 = 3636.85$.

To simulate adipose tissue, a finite element model was created. The average elastic and shear modulus for strain rates ranging from 0.05 to 5% were determined to be: Initial $E \approx 12.71 \pm 10.93$ kPa, final $E \approx 1300 \pm 66.60$ kPa. Initial modulus of rigidity $G \approx 4.23 \pm 2.30$ kPa, final $G \approx 433.30 \pm 22.20$ kPa. For the Ogden and quasilinear viscoelastic models, the correlation coefficients were $R^2 = 0.9809$ and $R^2 = 0.9986$, respectively. When comparing the model to the experimental data at a 0.5% strain rate, these were the coefficients of determination. A comparison of experimental and simulation results revealed that the QLV model could reproduce the stress-strain curve with acceptable accuracy.

[1] College of Mechanical and Vehicle Engineering, Hunan University, Changsha, 410082, China.
[2] Department of Advanced Materials and Technologies, Faculty of Material Science, Politechnika Slaska, 40-019 Katowice Poland.
[*] Corresponding author benard.kipsang@polsl.pl.

Under steady loading, it was discovered that subcutaneous adipose tissue is strain rate dependent and exhibits a non-linear stress-strain response. Because it is soft and compliant under quasi-static loading but stiff and resilient under dynamic loading, it exhibits both viscous and elastic behavior.

16.1. Introduction

Technology advancement has not only helped to improve counterterrorism measures, but it has also enabled insurgent bomb makers to develop new, more sophisticated explosives used on battlefields to attack. Blast injuries are more common than not encountered on battlefields. In such a blast situation, severe injuries are frequently accompanied by traumatic effects throughout the body. Post-traumatic effects, such as ear injuries, lung injuries, abdominal injuries, brain injuries, and soft tissue damage, occur more frequently than death [1].

A blast wave is generated from an explosion by the sudden release of a large amount of energy in a very small volume. A blast wave is commonly comprised of a shock wave and blast wind [2]. When a bomb explodes, the area around the explosion becomes over-pressurized, resulting in highly compressed air particles that travel faster than the speed of sound. This wave will dissipate over time and distance and will exist only for a matter of milliseconds. This initial blast wave inflicts the most damage. When this blast wave reaches a human body, the body will feel the force of the blast, which is the primary and initial impact of the shockwave [3]. This damages the body on impact. The force with which a blast occurs is called its load. Blast loading can inflict enough stress on the body to cause it to be flung onto a structure. After a blast wave strikes the body, high-velocity shockwaves, or stress waves, will continue to pass through it. Then travel through the organs and tissues. Shockwaves carry energy through the medium they pass through; they're supersonic and transport more energy than sound waves. At the explosion site, a vacuum is created by the rapid outward movement of the blast. This vacuum will almost immediately refill itself with the surrounding atmosphere. This creates a very strong pull on any nearby person or structural surface after the initial push effect of the blast has been delivered. As this void is refilled, it creates a high-intensity wind that causes fragmented objects, glass and debris to be drawn back in toward the source of the explosion [3]. Therefore,

in a blast scenario, two parts namely positive and negative sections are created. Blast wave leads to injury through spalling, implosion, and inertia [4].

Blast injuries have been categorized into four major types: primary, secondary, tertiary and mutilating [2, 4, and 5]. Primary blast injury is caused by a blast wave striking the body and transmitting energy directly into the body. Currently, there are no effective ways to prevent shockwaves from passing through protective clothing, and in some cases protective measures may even amplify the destructive effects [6]. Secondary blast injury occurs by debris propelled onto or into the body by the blast or its blast wave. The most common cause of death in a blast event is secondary blast injuries. These injuries are caused by flying debris generated by the explosion. Terrorists often add screws, nails, and other sharp objects to bombs to increase injuries. Soft tissue injuries are one of the most common types of secondary blast injuries. Thus, it is of substantial interest in this research.

Following blast dynamics, Personal protection equipment (PPEs) have continually been designed. However, to date, military-grade armor materials designed to mitigate ballistic and shrapnel attacks are less effective in resisting blast impacts. In order to improve blast absorption characteristics of armors, the first key step is thoroughly understanding the effects of blasts on the human body itself. In literature, an extensive study on the effects of blast on some parts of a human body has been conducted using experimental and computational modeling techniques. Abundant computational models to study blast effects on the human head were developed by Ganpule et al. [7, 8]. Arnab Chanda et al. modeled skin and bone sections from six locations of the body i.e. the elbow, figure, wrist, cheek bone, forehead and skin basing on the knowledge of human anatomy and eye estimation of three subjects [1]. Subcutaneous adipose tissue, like other soft tissues in human body, is vulnerable to blast loading and shrapnel penetrations among other impacts. Furthermore, studies have shown that subcutaneous adipose tissue plays an important role as a mechanical load absorbing and distributing member that absorbs shock and protects against local stresses [9, 10]. However, there is a paucity of studies characterizing biomechanical response of adipose to loading conditions. This provides adequate grounds to study the mechanics of adipose tissue loading, which will be a vital step towards improving the design of protective devices.

Most experiments have been conducted on surrogates, animal models, cadavers and few on live human subjects [10, 11]. Adipose tissue is commonly characterized using human heel pad tissue, human breast and porcine subcutaneous [9–11] whereby its

biomechanics have been studied experimentally and numerically using finite element methods. In this case, a pig's subcutaneous adipose tissue specimen was used as a model for studying human subcutaneous tissue because comparatively, pigs have genetical, physiological and anatomical traits similar to humans, which make them one of the most useful and versatile animal models. Owing to these similarities, data generated from porcine models are more likely to lead to viable human treatments than those from murine work. In addition, the similarity in size and physiology to humans allows pigs to be used for many experimental approaches not feasible in mice. Research areas that employ pigs range from neonatal development to translational models for cancer therapy [30]. Specimen(s) were subjected to varying strain rates [10–12] to demonstrate different loading conditions. Adipose, as with most biological tissues, exhibits heterogeneous, rate-dependent, viscoelastic behavior and experiences large non-linear deformations [15]. It is suggested that adipose is approximately isotropic in structure and due to the large lipid content, is almost incompressible [11]. Notwithstanding, a recent study by [14] observed some anisotropy in the specimen.

This work aims to future look into adipose tissue mechanics by investigating its mechanical properties under quasi-static and dynamic compression loading at varying strain rates so that important factors that affect its physical properties are understood. Thus, give an insight into predicting the behavior based on the components it is made of.

16.2. Materials and methods

MTS machine was used to perform the uniaxial compression hence obtaining the stress versus strain response data of porcine fat tissue from the material testing mechanical laboratory.

16.2.1. Specimen preparation and Experimentation

A pig's subcutaneous adipose tissue was obtained from the nearby market, fresh and succulent with the skin on. The skin was dissected off the adipose tissue using a scalpel blade so that preloading conditions are not altered much by the cutting force. More so, correct measurements and the right shape are maintained on the surfaces of the specimen. This was to ensure the consistency of all the samples. The resulted

block of adipose was cut accurately into cubes of 10mm in dimensions. The measurement of dimensions in the specimens' unloaded state was done using a conventional ruler. To enable the generation of data consistent with the specified specimen shape, the dimensions of every specimen were confirmed prior to loading.

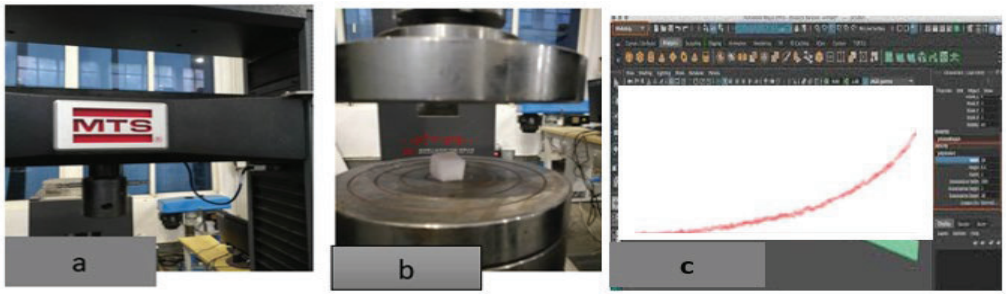

Fig. 1. (a) MTS universal testing machine (b) Specimen placement (c) Computer data generation and plotting
Rys. 1. (a) Uniwersalna maszyna wytrzymałościowa MTS (b) umieszczenie próbki (c) generowanie i komputerowe kreślenie danych

The specimen was placed on the center of the lower platen and oriented so its remaining four surfaces were perpendicular to both the platens. This allows the compression to be uniaxial without limiting shear loading because the test was unconfined. The upper platen was lowered down to partially touch the top surface of the specimen. This point was assumed to be the datum. The two platens were made sure that they were frictionless to avoid lateral stresses. A compressive loading regime was programmed into the software i.e. zero load, zero position and find contact. The test was executed using the software program where the sample was loaded under compression. These tests were performed over 3 strain rate regimes which is 0.05%, 0.5% and 5%. The same procedure was followed for all the specimens. The ambient temperature was 10°C.

It was assumed that the experiment occurred under symmetric conditions, with a homogeneous, isotropic and incompressible material, and that imposed deformations were small compares to the original size of the cubic specimen.

16.2.2. Experimental data analysis

The experimental engineering stress was found by dividing the reaction force at every sample point by the un-deformed contact area. The engineering strain corresponded to the displacement of the platen divided by the un-deformed (original) height of the specimen. Nominal stress and strain were also calculated.

Unlike traditional solid materials that are typically described with a linear elastic or hyperelastic behavior, most soft tissues are inhomogeneous, anisotropic, and frequently have integral nonlinear viscoelastic mechanical behavior because they consist of significant amounts of interstitial fluids. Therefore, this mechanical behavior involves a response that changes with time as a product of tissue relaxation. All the above-mentioned characteristics together with a nonlinear stress-strain relationship make the characterization of biological tissues complicated [23]. Three--term QLV and one-tern Ogden models were selected for modeling the passive behavior of subcutaneous adipose tissue. The equation below expresses the Ogden hyperelastic material law.

$$W = \sum_{i=1}^{n} \frac{\mu_i}{\alpha_i}\left(\lambda_1^{\alpha_i} + \lambda_2^{\alpha_i} + \lambda_3^{\alpha_i} - 3\right) + K(J - 1 - InJ) \quad (1)$$

Where W is the strain energy of the model, **μ** is the initial shear modulus, **α** is the strain hardening exponent, **λ_i** is the stretch ratio in three directions: **x**, **y** and **z** and **J** represents the bulk modulus. Subcutaneous AT was considered incompressible, in this way, **J** equals to 1. Consequently, one-order Ogden law simplifies a can be expressed as follows,

$$W = \frac{2\mu}{\alpha^2}(\lambda_1^{\alpha} + \lambda_2^{\alpha} + \lambda_3^{\alpha} - 3) \quad (2)$$

Quasilinear viscoelastic (QLV) constitutive model is perhaps the most common viscoelastic constitutive model used to characterize biological soft tissues. It has the capability of modeling materials with time-dependent viscoelastic behavior that undergo large deformation. The constitutive equation, which is defined as the convolution integral of the time-dependent reduced relaxation function with the time derivative of the elastic response function, can be used to fit the experimental data and to estimate the QLV parameters [25, 26].

QLV theory models the viscoelastic response of a material based on a stress relaxation function and the instantaneous stress resulting from a ramp strain as:

$$\sigma(t) = G(t) * \sigma^{e}(\varepsilon) \quad (3)$$

Where **σ (t)** is the stress at any time **t**, **$\sigma^e(\varepsilon)$** is the stress corresponding to an instantaneous strain, **G(t)** is the reduced relaxation function representing the stress of the material divided by the stress after the initial ramp strain noted that * represents

the convulsion of **G** and $\boldsymbol{\sigma^e(\varepsilon)}$**,** which is **G(t)** multiplied by $\boldsymbol{\sigma^e(\varepsilon)}$ and then integrated over time. **G(t)** is defined as:

$$\mu\alpha G(t) = \frac{\sigma(t)}{\sigma(0^+)} \; and \; G(0^+) = 1 \tag{4}$$

The complete stress history at any time is then the convolution integral:

$$\sigma(t) = \int_{-\infty}^{t} G(t-\tau) \; \frac{\delta\sigma^e(t)}{\delta\varepsilon} \frac{\delta\varepsilon}{\delta\tau} \tag{5}$$

Where G is the reduced relaxation function, $\frac{\delta\boldsymbol{\sigma}^e(\mathbf{t})}{\delta\varepsilon}$ represents the instantaneous elastic response, and $\frac{\delta\varepsilon}{\delta\boldsymbol{\tau}}$ is the strain history. It can be assumed that t starts at zero instead of negative infinity for the exponential situation. The reduced relaxation function is:

$$G(t) = ae^{-bt} + ce^{-dt} + ge^{-ht}$$

Or
$$G(t) = \sum_{i=1}^{n} G_i e^{\beta_i t} \tag{6}$$

Where **a**, **b**, **c**, **d**, **g**, **h** are all constants to be determined experimentally. $\boldsymbol{\beta_i}$ is the decay constant.

The instantaneous stress response is assumed to be represented through the nonlinear elastic relationship:

$$\sigma^e(\varepsilon) = A(e^{B\varepsilon} - 1) \tag{7}$$

In the nonlinear elastic function, **A** and **B** are constants that must be determined by experiment. They are also constants to be fit with experimental data. Three terms of coefficients are adopted in this study.

16.2.3. Analytical solution

To determine the strain rate dependent material properties, an inverse FE algorithm was used. Selected models (Ogden and QLV) were simulated numerically in python using the available package weave namely: matplotlib, numpy and scipy. Parameter optimization was carried out using a pycham optimization package. Thus, material parameters were calibrated by minimizing the square of the absolute error between the stress-strain data obtained numerically with the experimental measurements. This

produced optimal material parameters. The use of absolute errors instead of relative errors is justified as it provides a better fit for large deformations [27]. Since the main output of numerical and experimental tests was the compressive force measured over time on the adipose tissue specimen by the load cell, the objective function was formed to calculate and minimize the difference between the experimental and numerical force measurements.

$$f(x) = \sqrt{\frac{\sum_{i=1}^{n}(y_{iExp} - y_{iNum})^2}{n}} \tag{8}$$

Where **f(x)** is the objective function, $\mathbf{y_{iExp}}$ is the value of experimental force, $\mathbf{y_{iNum}}$ is the responsive numerical force and **n** is the number of data points in experimental tests.

Hyperelastic material parameters; **μ**, **α**, **C1, C2,** and **C3** were obtained from the numerical inverse process.

16.2.4. Modelling and Simulation

Commercial solver LS-DYNA_SMP_R11.0.0×64 was used in conjunction with Ls-prepost(R) V4.5.24 for modeling and simulations of the adipose tissue. Ls-prepost can be used to model simple components that do not have intricacies in its parts. This version of the software have Implicit and Explicit finite element codes.

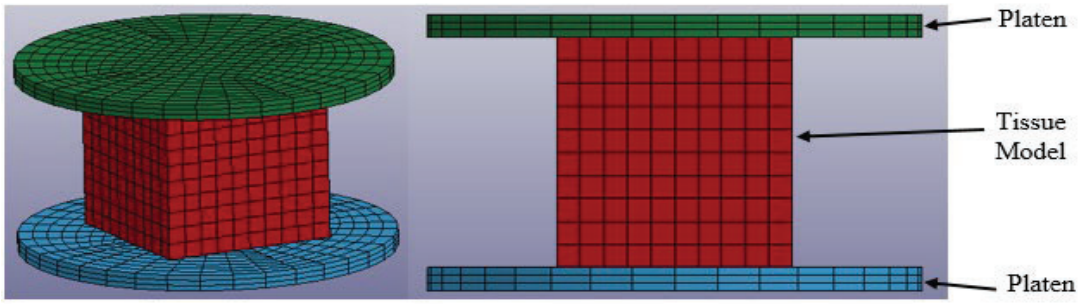

Fig. 2. Adipose tissue model between two steel platens
Rys. 2. Model tkanki tłuszczowej pomiędzy dwiema stalowymi płytami

The model was meshed to obtain accurate results. Automatic surface to surface contact type was chosen with segment sets between the slave and/or master and the specimen. Static coefficient of friction (FS) was set to 0.01 for both cases.

16.2.5. Boundary conditions

The model setup is that all translational and rotational degrees of freedom (DOF) about the bottom platen are constrained while on the top platen, the translational DOF in compression direction was unconstrained. This allows the top platen to move downwards during compression. The specimen model remains unconfined in the middle of the top and bottom platens thus, undergoing uniaxial compression. To execute the compression work, top platen (slave) was given a prescribed motion of 0.5%/s and the load curve scale factor set to negative 1.

16.2.6. Hyperelastic Material models

Ls-dyna present material models that can be used to analyze biological materials. However, few can reasonably be used to analyze the constitutive properties of adipose tissue. The models that can be used for this particular one are: MAT_077-O OGDEN_RUBBER and MAT_176 QUASILINEAR_VISCOELASTIC.

The former is a hyperelastic nearly incompressible model in principal directions and the latter is a quasi-linear, isotropic, viscoelastic material which represents biological soft tissues, such as the brain. Therefore suitable for simulating adipose tissue because it undergoes finite deformation when stressed.

16.2.7. Inverse finite element method/analysis

To implement finite element analysis in ls-dyna, material parameters found experimentally were input into the respective material models. Ogden material model (Fig. 4) required the input of parameters: density of material, Poisson's ratio, mu (μ), alpha (α) and optional relaxation shear modulus (G) and relaxation constant(s) (β). QLV material model (Fig. 5) required: density of material, Poisson's ratio, bulk modulus, relaxation shear modulus (G) and relaxation constant(s) (β) and elastic constants C_1, C_2 & C_3. The experimentally acquired parameters can be substituted with load curve ID in the material model keyword cards.

Table 1

Parameters input to material model cards

Density (ρ)	**920 kg/cm^3**
Poisson's ratio (υ)	0.499983
Bulk modulus (k)	5e5 Pa
Relaxation shear modulus (G)	$G_1 = 3000$, $G_2 = 2770$
Relaxation constants (β)	$\beta_1 = 310$, $\beta_2 = 100$
Ogden parameters	$\mu = 16.40$, $\alpha = 8.410$
QLV parameters	$C_1 = -136.98$, $C_2 = -225.60$, $C_3 = 3636.85$

The parameter values of ρ, υ, G_1 and β_1 used above were obtained from [46] simulation of the calibration experiment with low strain rate (0.2%/s).

During the simulation, the specimen was compressed at a strain rate of 0.5%/s until 50% of its initial length as demonstrated in Fig. 3 below. Ogden model simulation was carried by invoking implicit solver while QLV simulation used explicit solver because it cannot be simulated in implicit solver. Both simulations converged successfully.

Stress-strain data from the elastic response of the material during simulation was obtained by plotting designated node(s) and/or element(s) stress-strain responses that were enabled by invoking in DATABASE_HISTORY_NODE/SOLID_ID. The data was saved to excel files for later analysis.

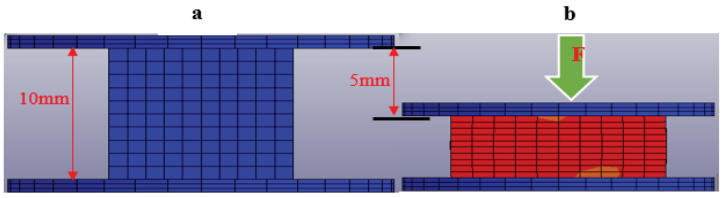

Fig. 3. (a) Tissue sample before compression (b) After compression
Rys. 3. (a) Próbka tkanki przed kompresją (b) po kompresji

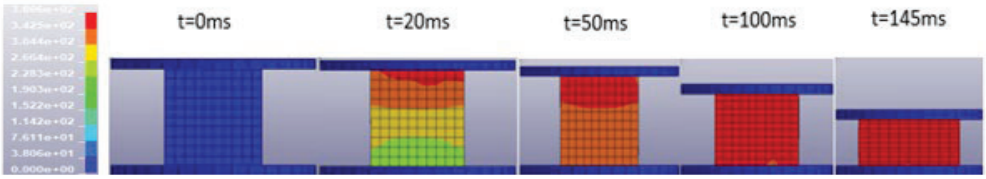

Fig. 4. Demonstrates simulation using Ogden material model
Rys. 4. Demonstracja symulacji z wykorzystaniem modelu Ogdena

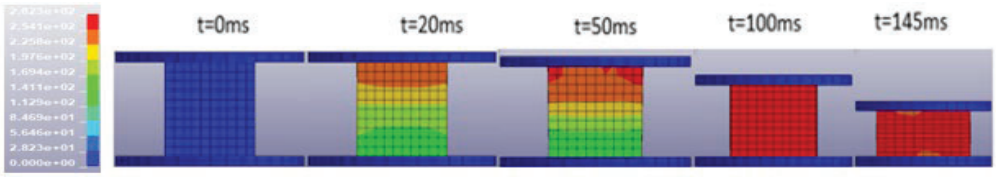

Fig. 5. Demonstrates simulation using quasilinear viscoelastic (QLV) material model
Rys. 5. Demonstracja symulacji z wykorzystaniem kwaziliniowego modelu lepkosprężystego

From the above demonstrations, it's observable that the material models respond to the applied load differently. This is depicted by change of stress colorations and shape with respect to time. Ogden model gives almost immediate response to the load compared with QLV model. On examining further, the specimen during the compression test, lateral elongation was observed proving the presents of Poisson's ratio in the material. Poisson's ratio contributes to the form of stress-strain diagram. The initial and final cross-sectional area of the specimen in compression changed. In this way, nominal and true strain diagrams cannot be identical. Until 50% compression, the volume of the material was conserved.

The experimental curve at 0.5%/s was chosen for comparison with the developed finite element model. The reason for choosing only one curve is that there is not always a continuous increasing stiffness from lower to higher strain rates within the levels, lower, intermediate and high of strain rate, hence one curve is sufficient. More curves would not increase the accuracy [27].

16.3. Results

16.3.1. Experimental results

Experimental data obtained from compression of adipose tissue (see Table 1 above) in the mechanical laboratory were represented graphically using OriginPro 2019b. It is a graphing and data analysis software. Curves of the three samples are plotted for each strain rate regimes i.e. 0.05/s, 0.5/s and 5/s as shown in Fig. 6 (a), 6 (b) and 7 (a) below.

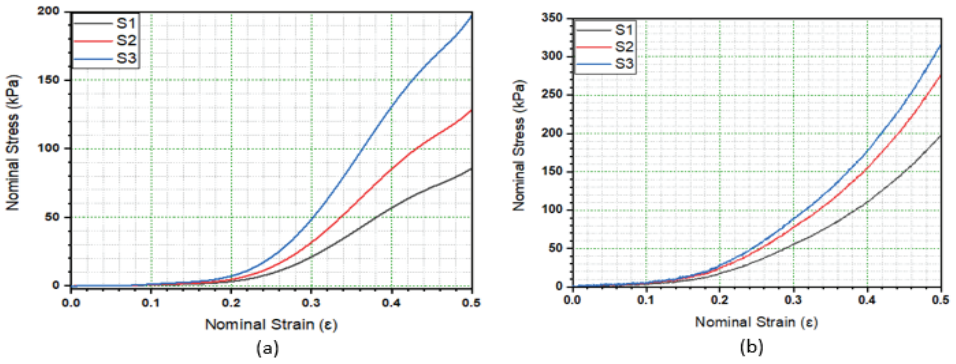

Fig. 6. (a) Three specimen samples at 0.05% strain rate. (b) Three specimen samples at 0.5% strain rate
Rys. 6. (a) Trzy próbki przy odkształceniu 0.05%. (b) Trzy próbki przy odkształceniu 0.5%

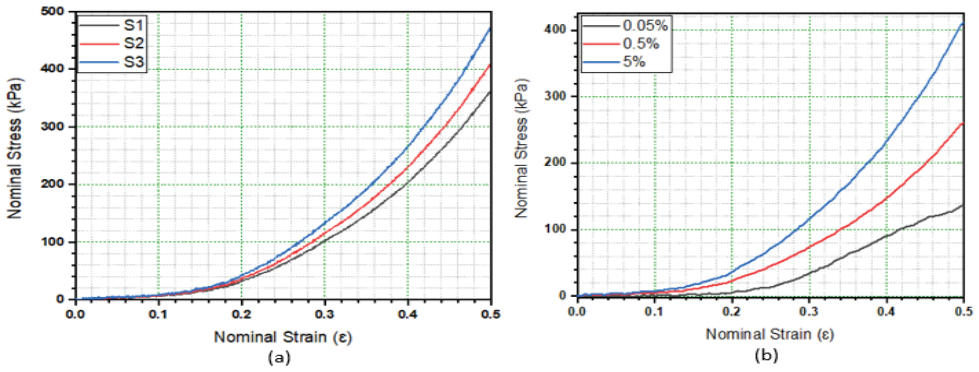

Fig. 7. (a) Three specimen samples at 5% strain rate. (b) Average of 0.05%, 0.5% and 5% strain rates from figure 6 (a), 6 (b) and 7 (a) respectively
Rys. 7. (a) Trzy próbki przy odkształceniu 5%. (b) Średnie dla odkształceń 0.05%, 0.5%, 5% z rysunków 6 (a), 6 (b) i 7 (a)

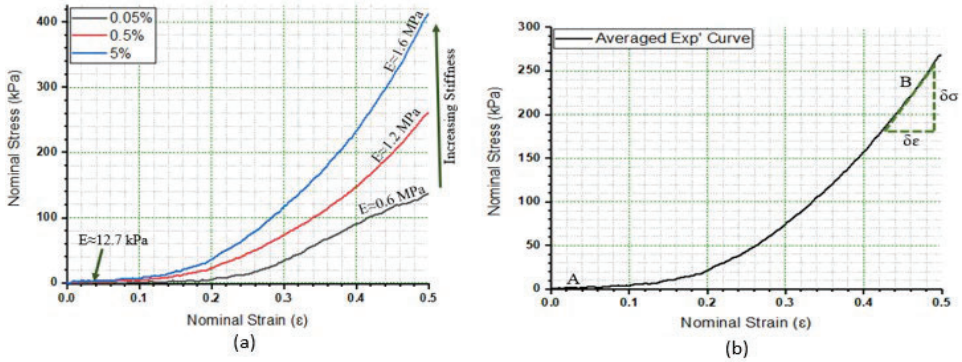

Fig. 8. (a) Increasing stiffness as strain rate increases. (b) Average from figure 3.3
Rys. 8. (a) Wzrastająca sztywność przy wzrastającym odkształceniu. (b) Średnia z rysunku 3.3

The values of elastic modulus and modulus of rigidity shown in the table below was obtained from calculating the slope of the curve in Fig. 8 (b) above.

Table 2

Average approximate elastic and shear modulus with standard deviations for strain rates between 0.05% and 5%

	Initial (A) (kPa)	**STD (kPa)**	**Final (B) (kPa)**	**STD (kPa)**
Elastic modulus (E)	12.71	10.93	1300	66.60
Shear modulus (G)	4.23	2.30	433.30	22.20

The graph describes the stress-strain relationship of the adipose tissue and more so clearly depicts the strain rate dependence of the tissue. The elastic modulus is within the range reported in [9, 11, 20, 21] and the shear modulus calculated from the curve slope is in agreement with the values reported in [11].

16.3.2. Analytical results

Using python algorithm parameters i.e. **μ**, **α** and $\mathbf{C_1}$, $\mathbf{C_2}$, & $\mathbf{C_3}$ from Ogden law and Quasilinear-Viscoelastic law respectively, are obtained as tabulated in Table 3 and 4 below.

Table 3

Ogden parameters for the listed strain rates

Strain Rates	μ	α	R^2	RMSE
0.05%	7.820	8.763	0.9973	2.090
0.5%	16.062	8.330	0.9870	8.804
5%	25.380	8.331	0.990	13.91

Table 4

QLV parameters for the listed strain rates

Strain Rates	C_1	C_2	C_3	R^2	RMSE
0.05%	-124.36	840.40	-15.280	0.990	4.251
0.5%	-32	593.20	1041.14	0.9993	2.032
5%	-51.11	937.26	1645.00	0.9993	3.210

Table 5

Averaged Ogden parameters

μ	α	R^2	RMSE
16.40	8.410	0.9809	11.195

Table 6

Averaged QLV parameters

C_1(-)	C_2(-)	C_3	R^2	RMSE
136.980	225.60	3636.85	0.9986	3.90

These averaged parameters are used in the respective material models for simulations.

16.3.3. Inverse FEM results

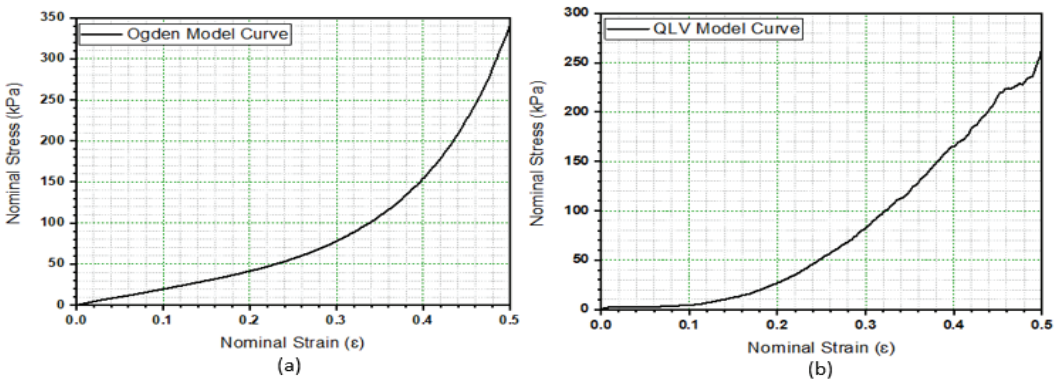

Fig. 9. (a) Stress-Strain response of Ogden material model. (b) Stress-Strain response of quasilinear viscoelastic material model

Rys. 9. (a) Krzywa naprężenie-odkształcenie dla modelu Ogdena. (b) Krzywa naprężenie-odkształcenie dla kwaziliniowego modelu lepkosprężystego

Ogden model depicts some sensitivity to applied load even from the beginning and increasingly non-linear from 0 to 0.5 Strain. According to ls-dyna material selector, Ogden material model is in the family of rubber (RB). This can explain the low viscoelasticity and stress sensitivity seen at initial stages of stress application as shown on Fig. 9 (a) above. Apart from the graphical representation, its stress-strain responses can be observed in Fig. 4.

QLV finite model curve shows pliability of the specimen during compression as seen in the graph above, from 0 to 0.1 strain. QLV material model is in the family of biological materials (BIO). Stress response of this model can also be described by Fig. 5.

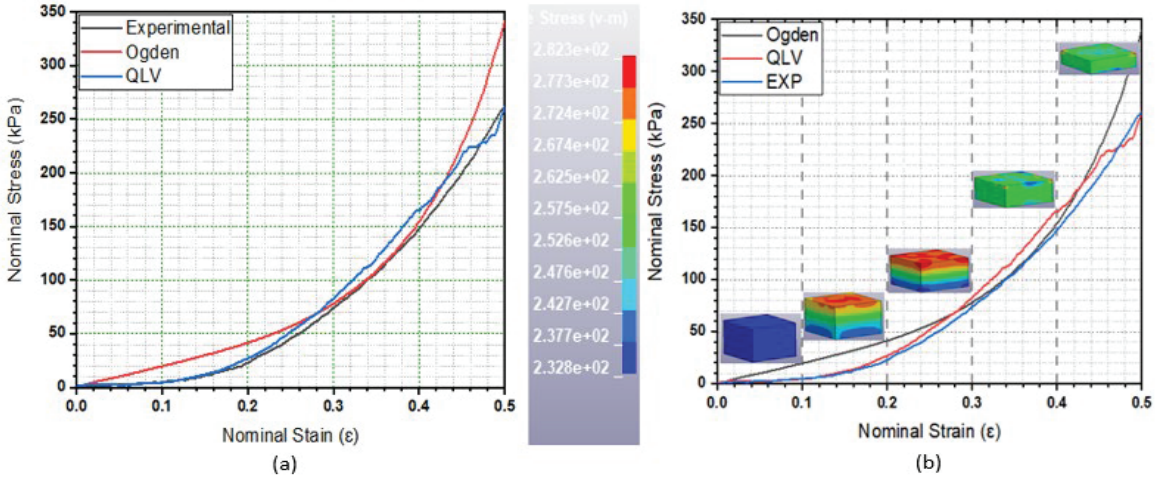

Fig. 10. (a) Experimental and finite element models data comparison. (b) Models deformation and curves under compression loading

Rys. 10. (a) Porównanie danych eksperymentalnych I modelu elementow skończonych. (b) Modele deformacji I krzywych pod obciążeniem ściskającym

A clear understanding of the relationship among model compression, load--deformation curves and effective stresses can be obtained from the figure below.

16.4. Discussion

Uniaxial compression test was conducted in the laboratory to obtain the stress-strain data when the specimen was subjected to three different loading rates as mentioned earlier on in the previous chapter(s). The compiled data were represented graphically to bring into perspective the stress-strain response when subcutaneous adipose is loaded at varying rates. Three specimen samples were tested at every strain rate. That is: 0.05%, 0.5% and 5%. At 0.05% strain rate, it is observed that the curves are less inclining and the stress for deforming the specimen to 50% of its initial shape is also low as shown by Fig. 6 (a). Curves at 0.5% strain rate are more inclined and its deformation stress is higher than the one for 0.05%. The slope of curves at 5%/s increased further than for the first two strain rates. The three samples in each strain rate are averaged into one as illustrated in Fig. 7 (b). These clearly show the stress--strain response with changing loading rate. The elastic modulus and stress strain

curve were found to be dependent on the strain rate. As the strain rate increases, the elastic modulus increases and the stress strain curve becomes stiffer.

The general behavior of the curve shows that from 0 to 0.1 strain, the material deforms with low sensitivity to the applied load - it remains viscous. From 0.1 to 0.2, sensitivity to loading rises. From 0.2 to 0.3, a sharp stiffness is observed and between 0.3 and 0.5, the material's stiffness increases significantly. This behavior gives a non-linear stress strain curve. The viscous behavior of subcutaneous adipose can be attributed to the 3D foam cell structure of interlobular septa and large amount of interstitial fluids that fill the spaces between cells. Whereas the elasticity is attributed to the existence of adipose ECM in varying degrees of stiffness and elasticity which is a property primarily dependent on collagen and elastin concentration(s). The combination of these properties yields a viscoelastic material that is manifested in adipose tissues.

Regression analysis was conducted on stress-strain data from experiment to obtain the constitutive hyperelastic parameters of the tissue. Ogden and QLV models were employed to characterize the hyperelastic properties and are presented in Table 5 and 6 respectively. Strain hardening exponents remained relatively same for all the strain rates. The value of shear response (μ) see table 3.2, depicts that the material's deformation behavior under steady loading is strain rate dependent because it increases with strain rate. The negative values of μ is attributed to artifacts of the fitting. It is magnified when some of the powers in the Ogden model are negative. In such case, a small but positive shear modulus can artificially appear as negative. This could be experienced more often when the material undergoes finite deformation. In this study, the values of μ were taken as positive. QLV elastic constants C_1, C_2 and C_3 were used as they are in material model keyword cards.

Stress-strain data from finite element model analysis were plotted. Ogden model and QLV model showed different responses during compression test, see Fig. 9 (a) and 9 (b) The major difference is that curve from Ogden data shows instant sensitivity to loading whereas QLV curve shows low sensitivity to loading initially as observed on experimental curves.

To validate the results of the experiment, the stress strain curve at a strain rate of 0.5%/s was compared to the stress strain curves from finite element simulation. As observed in Fig. 10 (a), there is a pronounced difference between Ogden curve and

experimental curve but slight difference between QLV and experimental curve. The correlation coefficients for Ogden and quasilinear viscoelastic models were $R^2 = 0.9809$ and $R^2 = 0.9986$ respectively.

A Comparison between the experimental and simulation results shows the capability of QLV model to reproduce the stress strain curve with acceptable accuracy. Therefore, the suggested material parameters are capable of fairly predicting the load and deformation of subcutaneous fat tissue.

16.4.1. Conclusions and recommendation

Subcutaneous adipose tissue is strain rate dependent and shows a non-linear stress-strain response under steady loading. It manifests both viscous and elastic behavior by the virtue that, it is soft and compliant under quasi-static loading but stiff and resilient under dynamic loading.

Quasilinear viscoelastic model gives a better prediction of the load-deformation response of subcutaneous fat tissue than Ogden. Model validation was performed employing the coefficients of determination in which the one for QLV nears 1 and its RMSE is small compared to Ogden.

A fresh sample of porcine can possibly give better results especially when all conditions are recorded prior to testing. Therefore, it is recommended that fresh samples be used in future to investigate the mechanical properties of subcutaneous adipose tissue so that comparative results can be obtained.

Credit author statement

Wesley C. Rutto: Conceptualization, Methodology, Investigation, Data collection, Data organization, Software, Visualization, and writing – Original draft preparation.

Benard Kipsang: Writing – Reviewing and Editing.

Conflict of interest

The author declares that the research was conducted in the absence of any relationships that can be interpreted as a potential conflict of interest.

Acknowledgements

We thank the Chinese government ministry of commerce (MOFCOM) for funding this research.

Bibliography

1. Effect of blasts on subject-specific computational models of skin and bone sections at various locations on the human body. Arnab Chanda 1, Rebecca Graeter 2, and Vinu Unnikrishnan 1, Published date 12 November 2015.
2. Ballistic helmets – Their design, materials, and performance against traumatic brain injury. S.G Kulkarni, X.-L. Gao, S.E. Horner, J.Q. Zheng, N.V. David (2013). US Army Research. 201.
3. TOM SCHEVE; How Bomb Blasts Cause Damage: howstuffworks 2008.
4. Zara R. Mathews, MD*, Alex Koyfman, MD†. The Journal of Emergency Medicine, Vol. 49, No. 4, pp. 573–587, 2015; BLAST INJURIES
5. Yan Zhao, Yuan-Guo Zhou*. The past and present of blast injury research in China; Available online 12 November 2015.
6. Christopher George Thom: Soft Materials under Air Blast Loading and Their Effect on Primary Blast Injury; Waterloo, Ontario, Canada, 2009.
7. Ganpule S.G., Chandra N., Salzar R., (2013): Mechanics Of Blast Loading On Post-Mortem Human Heads in The Study Of Traumatic Brain Injury (TBI) Using Experimental And Computational Approaches [PhD Dissertation]: University of Nebraska-Lincoln, 289.
8. Ganpule S., Chandra N., (2013): Mechanics of Interaction of Blast Waves on Surrogate Head: Effect of Head Orientation. ASME 2013 Summer Bioengineering Conference: American Society of Mechanical Engineers, V01BT55A028-029.
9. Alkhouli N., Mansfield J., Green E., Bell J., Knight B., Liversedge N., Tham J.C., Welbourn R., Shore A.C., Kos K., Winlove C.P., (2013): The mechanical properties of human adipose tissues and their relationships to the structure and composition of the extracellular matrix.
10. Thomas Payne, Sean Mitchell, Richard Bibb, Mark Waters; 30 September 2014; the evaluation of new multi-material human soft tissue simulants for sports impact surrogates.
11. Kerstyn Comley, Norman Fleck, (2012): The compressive response of porcine adipose tissue from low to high strain rate.

12. Grigoris Grigoriadis, Nicolas Newell, Diagarajen Carpanen, Alexandros Christou, Anthony M.J. Bull, Spyros D. Masouros; 8 September 2016; Material properties of the heel fat pad across strain rates.
13. Bruno Bordoni, DPT, DO, PhD,[1,2,3] Fabiola Marelli, DPT, DO,[2,3] Bruno Morabito, DPT, DO, PhD,[2,3] and Roberto Castagna, DPT, DO[2]; A New Concept of Biotensegrity Incorporating Liquid Tissues: Blood and Lymph
14. Sommer G., Eder M., Kovacs L., Pathak H., Bonitz L., Mueller C., Regitnig P., Holzapfel G.A., (2013): Multiaxial mechanical properties and constitutive modeling of human adipose tissue: a basis for preoperative simulations in plastic and reconstructive surgery. Acta Biomater. 9 (11), 9036–9048.
15. Sapozhnikov S., Ignatova A., (2013): Experimental and theoretical investigation of deformation and fracture of subcutaneous fat under compression. Mech. Compos. Mater., 48 (6), 649–654.
16. Peckham M.: Extracellular Matrix – 'Ground substance'. Faculty of Biological Sciences, University of Leeds.
17. Assist. Prof. Dr. Pınar Tulay, Ph.D. (Molecular biology of THE CELL). Extracellular Matrix (ECM) and Mechanisms of Cell Communication. Faculty of Medicine Near East University.
18. Mithieux S.M., Weiss A.S., (2005): Elastin. Advances in protein chemistry, 70: 437–61.
19. G.A. Holzapfel (Paper No. 7 November 2000). Biomechanics of Soft Tissue
20. Azar F.S., Metaxas D.N., Schnall M.D., (2002): Methods for modeling and predicting mechanical deformations of the breast under external perturbations. Med. Image Anal. 6 (1), 1–27.
21. Samani A., Zubovits J., Plewes D., (2007): Elastic moduli of normal and pathological human breast tissues: an inversion- technique-based investigation of 169 samples. Phys. Med. Biol., 52 (6), 1565–1576.
22. Deepak-Kumar, (2015): Mathematical Modelling of soft Biological Tissues. Department of Mechanical Engineering Indian Institute of Technology.
23. Carlos Bustamante-Orellana, Robinson Guachi, Lorena Guachi-Guachi, Simone Novelli, Francesca Campana, Fabiano Bini, Franco Marinozzi, (2019): Biomechanics of Soft Tissues: The Role of the Mathematical Model on Material Behavior.
24. Cees W.J. Oomens, Gerrit W.M. Peters, (2017): Skin Mechanics. Hyperelastic models – Biomechanics of Living Organs.

25. Christian Quaia, Howard S. Ying, Lance M. Optican, (2010): The Viscoelastic Properties of Passive Eye Muscle in Primates. III: Force Elicited by Natural Elongations.
26. Elizabeth Mesa-Múnera, Juan F. Ramírez-Salazar, Pierre Boulanger, John W. Branch, (2012): Inverse-FEM Characterization of a Brain Tissue Phantom to Simulate Compression and Indentation.
27. Kristofer Engelbrektsson, (2011): Evaluation of material models in LS-DYNA for impact simulation of white adipose tissue. Master's Thesis in Solid and Fluid Mechanics. Department of Applied Mechanics. Chalmers University of Technology SE-412 96, Goteborg Sweden.
28. Cato T. Laurencin, Yusuf Khan, (2013): Regenerative Engineering. Text book.
29. Mei Song, Yi Liu, Ling Hui, (2017): Preparation and characterization of acellular adipose tissue matrix using a combination of physical and chemical treatments. 138–146. https://doi.org/10.3892/mmr.2017.7857
30. Schook L.B., Collares T.V., Darfour-Oduro K.A., De A.K., Rund L.A., Schachtschneider K.M., Seixas F.K.: Unraveling the swine genome: implications for human health. Vol. 3:219–244 (Volume publication date February 2015).

INVESTIGATION OF ADIPOSE MECHANICAL PROPERTIES UNDER COMPRESSION LOADING FOR IMPROVING HUMAN BODY ARMOR MODELING

Abstract

Adipose tissue mechanical properties were investigated under quasi-static and dynamic compression loading at varying strain rates on specimens made from porcine subcutaneous adipose tissue. The specimens were subjected to a uniaxial compression test to obtain stress versus strain response data. The tests were carried out at three strain rates: 0.05, 0.5, and 5%/s. For modeling three-term, QLV and one-term Ogden models were chosen. Python was used to numerically simulate experimental data. The hyperelastic material parameters obtained were as follows: $\mu = 16.4$, $\alpha = 8.4$, $C_1 = -137$, $C_2 = -225.6$, and $C_3 = 3636.85$ To simulate adipose tissue, a finite element model was created. The average elastic and shear modulus for strain rates ranging from 0.05 to 5% were determined to be: For the Ogden and quasilinear viscoelastic models, the correlation coefficients were $R^2 = 0.9809$ and $R^2 = 0.9986$, respectively. When

comparing the model to the experimental data at 0.5% strain rate, these were the coefficients of determination. A comparison of empirical and simulation results revealed that the QLV model was capable of reproducing the stress-strain curve with acceptable accuracy. Results showed that subcutaneous adipose tissue is strain rate dependent and exhibits a non-linear stress-strain response. It was found to be soft and compliant under quasi-static loading but stiff and resilient under dynamic loading, it exhibits both viscous and elastic behavior.

Keywords: subcutaneous adipose tissue, strain rates, finite deformation, viscoelastic, uniaxial compression, ls-dyna